Composite Structures 140 (2016) 630–643

Contents lists available at ScienceDirect

Composite Structures

journal homepage: www.elsevier.com/locate/compstruct

Lightweight design of automotive composite bumper system using modified particle swarm optimizer

Zhao Liu, Jiahai Lu, Ping Zhu *

State Key Laboratory of Mechanical System and Vibration, Shanghai Jiao Tong University, Shanghai 200240, PR China
Shanghai Key Laboratory of Digital Manufacture for Thin-walled Structures, Shanghai Jiao Tong University, Shanghai 200240, PR China

ARTICLE INFO

Article history:
Available online 4 January 2016

Keywords:
Composite bumper beam
Particle swarm optimization
Kriging
Structure optimization
Finite element simulation

ABSTRACT

Considering the crashworthiness and lightweight requirements in automotive industry, composite materials have been gaining increasingly more attention for their high specific strength, high specific stiffness and high energy absorption capability. Bumper system is one of the main structures which protect cars from the front and rear collisions. It is an effective way to develop the bumper system using composite materials to meet the crash safety and lightweight demands simultaneously. However, the application of composite material also introduces great challenges into the optimization design process, such as complex non-linear material behavior, multi-working conditions and large amount of design variables. In this paper, a structure design and optimization method is proposed for a commercial front bumper system made by carbon fiber woven composite. An integrated bumper system structure is presented considering the manufacturing process of composite material. Then, an optimization procedure incorporating the Kriging modeling technique and a modified PSO algorithm is proposed to find the optimal combination of design variables. The real vehicle experiment proves that the optimized bumper system meets all the requirements on strength and crashworthiness while with 31.5% weight reduction. The results reveal that the proposed design method is an efficient and effective way for composite structure design.

1. Introduction

Automotive crashworthiness is regarded as one of the most important design considerations [1–4]. In most of the collision accidents, bumper system is the first vehicle component involved in the impact and protects the car body and passengers to a certain extent. It is expected to be deformable enough to absorb the impact energy while possessing sufficient strength and stiffness to protect its nearby components [5]. Furthermore, with increasing need for energy conservation and environmental protection, lightweight design of vehicle structure has gained more and more attention in automotive industry [6]. Generally, material replacement, structural optimization method and advanced manufacturing technology can be employed during the lightweight design process, in which material replacement is regarded as the most effective approach. When incorporating weight saving and crashworthiness requirements for developing automotive safety components, such as the bumper system, composite materials have been gaining increasingly more attention for their high specific strength, high specific stiffness and high energy absorption capability. As a class of typical composites, fiber reinforced plastic (FRP) has been widely adopted to reduce the weight of the vehicle structure [7].

However, the application of composite materials also introduces a great challenge into the optimization design process, such as complex non-linear material behavior, multi-working conditions and large amount of design variables. Hosseinzadeh et al. [8] investigated a bumper beam system made of glass mat thermoplastic. The structure of the bumper beam was designed and verified based on the finite element analysis method considering the low-velocity impact performance. Davoodi et al. [9] focused their attention on improving the performance of a car bumper system using a hybrid kenaf/glass fiber composite. The results showed the benefits of using hybrid natural fiber in structural components of a car. Davoodi et al. [10] and Belingardi et al. [11] paid their attentions on selecting the best geometrical parameters of bumper structure to fulfill design requirements. Belingardi et al. [5] developed an integrated crash box and bumper beam system which had better crashworthiness. Major parameters, such as impact energy, peak load, energy absorption and so on were employed as evaluation criteria. The effectiveness of the proposed structure

* Corresponding author at: State Key Laboratory of Mechanical System and Vibration, Shanghai Jiao Tong University, Shanghai 200240, PR China. Tel./fax: +86 21 34206787.
E-mail address: pzhu@sjtu.edu.cn (P. Zhu).

http://dx.doi.org/10.1016/j.compstruct.2015.12.031
0263-8223/

was interpreted by finite element simulations. Although previous researchers have put forward some effective composite bumper versions, the optimization concept has not been incorporated into the design process because of large amount of design variables, multi-working conditions and high computational cost.

For a composite bumper system, both geometrical parameters and material parameters can be included as design variables. The geometry parameters can be decomposed into shape variables, for instance the size of the cross-section, and thickness variables. The material parameters consist of laminate stacking sequence, types of the fiber, reinforcement percentage, and so on. It is too complicated and difficult to consider all the parameters concurrently in the optimization procedure. Multi-load cases and associated high computational cost also restrain the proceeding of the structural optimization design, especially for crash conditions with high-nonlinearity performance and fragmentation absorption mechanism. In contrast to metallic materials, laminated composites possess more distinctive failure modes than metals [12–14], which result in high complexity of structural optimization design of CFRP components.

In this paper, experimental work is firstly conducted to obtain the mechanical properties of the studied carbon fiber plain weave composite. Based on the tested results, constitutive model considering tension/compression asymmetry and anisotropy is proposed with experimental verification. Then, considering the characteristic of the studied composite material and manufacturing process, an integrated bumper system structure is presented. After that, an optimization procedure incorporating the Kriging modeling technique and a modified PSO algorithm is proposed to find the optimal combination of both the shape and thickness variables. Real vehicle experiments are conducted to verify the optimal design of the bumper system.

2. Material characterization tests

2.1. Material properties

The material used in the present study is carbon fiber plain weave composite. Its fiber is TC33 carbon fiber made by Tairyfil Corporation. The matrix material is LY1564 SP/Aradur3486 from Huntsman, in which LY1564 SP is implemented as the resin and Aradur3486 as the hardener. The fabric is prepared as plain weave pattern with 3 k fibers in a tow. The basic properties of the carbon fiber and the matrix are presented in Table 1.

Composite sheets are manufactured by vacuum infusion process with a curing time of 5 h at 80 °C. The weight fraction of carbon fiber is 55%. The mechanical properties of the composite material under both quasi-static and high strain rate are given in Table 2. Quasi-static tensile test at the axial direction was conducted according to ASTM D638, and shear test according to ASTM D3518. For there are no consistent standards on dynamic tensile and shear tests, specimens for dynamic tensile and shear tests were conducted according to the requirement of testing equipments and recommendations of literatures [15]. For compression tests, even though standard specimen was recommended in ASTM D3410 for quasi-static test, cubic specimen was most frequently applied for both quasi-static and dynamic tests [15,16]. In the present study, the cubic specimen was designed according to the requirement of test equipment. Configurations of specimens were shown in Fig. 1. Due to the reinforcement type, the transverse direction properties are considered to be identical to the longitudinal ones. Thus, experiments were only conducted at 0° direction.

Table 1
Basic properties of the carbon fiber and the matrix.

Constituent	Type	Tensile strength [MPa]	Elongation [%]	Tensile modulus [GPa]	Density [g/cm^3]
Carbon fiber	TC33	3450	1.5	230	1.8
Matrix	LY1564/ Aradur3486	70–80	4.0–5.0	3.0–3.2	1.0–1.1

From the results, it can be seen that the in-plane mechanical properties of the studied carbon fiber woven composite show apparent tension/compression asymmetry and anisotropic characteristics. The strain rate also has an effect on the in-plane mechanical properties of the composite. The large difference of mechanical properties between tension and compression may be caused by tension/compression asymmetry characteristics of the carbon fiber and different failure patterns under the tensile and compressive loading conditions [15,17].

In order to predict the material strength under different strain rates, the following two phenomenological models are applied to quantify the strength property within the considered strain rate range:

$$\sigma_d = \sigma_s(1 + C_1 \exp(\log_{10}(\dot{\varepsilon})) + C_2(\exp(\log_{10}(\dot{\varepsilon})))^2 + C_3(\exp(\log_{10}(\dot{\varepsilon})))^3) \quad (1)$$

$$\sigma_d = \sigma_s\left(1 + C_1 \ln\left(\frac{\dot{\varepsilon}}{\dot{\varepsilon}_0}\right) + C_2\left(\ln\left(\frac{\dot{\varepsilon}}{\dot{\varepsilon}_0}\right)\right)^2 + C_3\left(\ln\left(\frac{\dot{\varepsilon}}{\dot{\varepsilon}_0}\right)\right)^3\right) \quad (2)$$

in which $\dot{\varepsilon}$ is the corresponding strain rate, and $\dot{\varepsilon}_0$ is the referential strain rate, which is defined as 0.001 s^{-1} here. Eq. (1) is used to fit the strength property of tension in the axial direction, while Eq. (2) is applied to the other two cases. Table 3 gives the fitted parameters. The precision of the fitted results is validated by the determination coefficient, R^2. Remarkable consistency can be observed between the fitted and experimental results.

2.2. Material constitutive model

In order to consider the effect of strain rate, tension/compression asymmetry and anisotropic characteristics, a user defined material model was established in this study.

For elastic condition, the stress–strain relationship is expressed in the anisotropic form as,

$$\begin{Bmatrix} \varepsilon_1 \\ \varepsilon_2 \\ \varepsilon_4 \end{Bmatrix} = \begin{bmatrix} \frac{1}{E_{11}} & -\frac{\nu_{21}}{E_{22}} & 0 \\ -\frac{\nu_{12}}{E_{11}} & \frac{1}{E_{22}} & 0 \\ 0 & 0 & \frac{1}{G_{12}} \end{bmatrix} \begin{Bmatrix} \sigma_1 \\ \sigma_2 \\ \sigma_4 \end{Bmatrix} \quad (3)$$

in which $E_1 = E_1^+$ when direction 1 is under tension, and $E_1 = E_1^-$ when under compression; $E_2 = E_2^+$ when direction 2 is under tension, and $E_2 = E_2^-$ when under compression.

In order to predict the loading capacity of composite structure, a strength criterion should be implemented to describe the failure of composite material. The World-Wide Failure Exercise [18] has tested the predictability of the most commonly used failure criteria based on identical experimental data and shown that all the tested failure criteria illustrated limited predictive accuracy for all the experimental results. Moreover, the experimental results are basically from unidirectional composite materials, which demonstrate much different mechanical performance from woven composites. Karkkainen et al. [19] and Mallikarachchi et al. [20] proved that under in-plane loading conditions, Tsai–Wu failure criterion can properly describe the failure of the woven composite. Thus, Tsai–Wu failure criterion is implemented in the present study.

The quadratic polynomial Tsai–Wu failure criterion under in-plane loading in stress form can be described as [21],

Table 2
Mechanical properties of the carbon fiber woven composite.

Loading condition	Mechanical properties	Strain rate			
		Quasi-static	200 s^{-1}	600 s^{-1}	1000 s^{-1}
0° tension	Modulus (GPa)	60.89 ± 1.71	59.23 ± 2.58	61.49 ± 5.83	61.35 ± 3.39
	Strength (MPa)	588.73 ± 52.18	609.20 ± 65.37	652.30 ± 85.49	723.63 ± 80.15
In-plane shear	Modulus (GPa)	3.14 ± 0.42	6.45 ± 0.68	6.07 ± 0.32	6.16 ± 0.75
	Strength (MPa)	48.43 ± 1.86	99.21 ± 2.31	117.05 ± 3.74	119.31 ± 5.86
0° compression	Modulus (GPa)	24.09 ± 0.15	39.83 ± 0.38	41.49 ± 0.27	40.49 ± 0.43
	Strength (MPa)	214.86 ± 4.37	490.76 ± 3.52	554.52 ± 3.07	564.43 ± 3.95

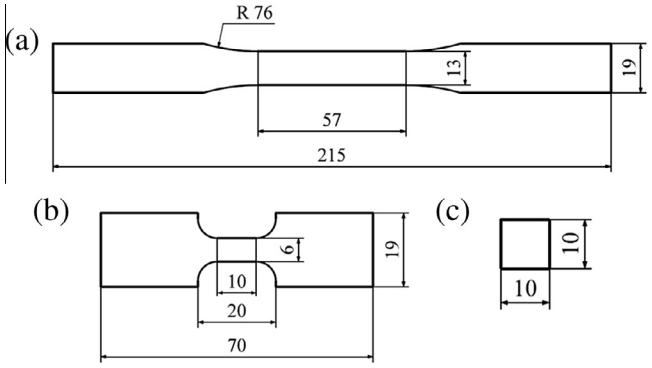

Fig. 1. Configurations of specimens for different loading conditions: (a) quasi-static tension; (b) high strain rate tension; (c) compression; (all dimensions are in mm).

Table 3
Fitted parameters of strain rate effect on strength property.

Loading condition	C_1	C_2	C_3	R^2
0° tension	9.77E−04	0	2.30E−05	0.9819
In-plane shear	4.74E−04	2.14E−03	4.11E−04	0.9957
0° compression	1.22E−04	7.78E−03	2.01E−05	0.9982

$$f_1(\sigma_1+\sigma_2)+f_{11}(\sigma_1^2+\sigma_2^2)+f_{44}\sigma_4^2+f_{12}\sigma_1\sigma_2=1 \quad (4)$$

in which f_i and f_{ij} represent failure coefficients such that Eq. (4) defines a failure condition when the equation is valid. The parameters f_i and the diagonal terms correspond to individual loading conditions in which only one stress resultant is non-zero; the non-diagonal terms deal with coupling effect between different stress resultants. The parameters can be obtained from properly designed experimental results. Thus, the parameters at the studied strain rates are illustrated in Table 4. The parameter f_{12} is based on approximation value [19,20]. Based on the fitted parameters in Table 3, Eqs. (1) and (2), the parameters used to describe the Tsai–Wu criteria under different strain rate can be calculated accordingly.

2.3. Experimental verification

In order to verify the accuracy of the material constitutive model, three-point bending and impact tests are conducted on rectangular composite tubes. The size of the tube for three-points bending is with 500 mm as the length, 100 mm and 50 mm as the width and height of the cross section, and 3 mm as the thickness. The size of the tube for drop weight test is with 180 mm as the length, 85 mm as the width of the cross section, and 2.5 mm as the thickness. The three-point bending test is carried out on the SANS test machine, and the impact test is carried out on the drop weight test machine at room temperature.

Numerical simulation of the three-points bending is performed in ABAQUS with the input material parameters given in Table 2. The material constitutive model described above is realized by the user subroutine UMAT of ABAQUS. The tube was meshed by shell element with 5 mm size. The contact between the tube and the support and compressor was defined by surface-to-surface algorithm with a friction coefficient of 0.2 [22]. Test and numerical simulation results of the three-points bending are illustrated in Fig. 2. Their force–displacement curves are compared in Fig. 3.

Numerical simulation of the drop weight impact test was performed in Ls-Dyna with the input material parameters given in Table 2. The material constitutive model described above was realized by the user subroutine VUMAT of Ls-Dyna. The tube was meshed by shell element with 5 mm size. The contact between the tube and rigid panel was defined by node-to-surface algorithm, and self contact was defined for the tube itself with the friction coefficient of 0.2. The element was deleted when all the integration points reach the failure criteria. Generally, considering the deformation pattern and energy dissipation mechanism as shown in Fig. 4a, multi-layer model is more accurate for composite material impact test than single-layer model [22,23]. However, the single-layer model is frequently adopted in structural performance simulations for efficiency consideration [24,25]. Thus, the single-layer simulation model is built for impact analysis. The test and numerical simulation results are illustrated in Fig. 4. Their deceleration–time curves are compared in Fig. 5.

From the results, it can be seen that for quasi-static loading conditions, the force–displacement curves of the three-points bending test and numerical simulation are very close. For impact test, the single-layer model underestimates the impact force to some extent as shown in Fig. 5. The error between the test and numerical results might be caused by applying the single-layer model instead of the multi-layer model for the former is impossible to model the inside frond as shown in Fig. 4a and b, thus, the energy dissipated by friction between the fronds and rigid panel is underestimated. The error may also be caused by the difference of the fiber volume fraction between the material for mechanical property tests and structure performance tests, which is introduced during the manufacturing process. However, the trends of the tested and predicted deceleration–time curves are close. Thus, the single-layer simulation method and the material constitutive considering the strain rate effect and tension/compression asymmetry can describe the material behavior of the carbon fiber plain weave composite properly, and can be applied to the finite element simulation.

Table 4
Strength parameters of the studied composite material.

Strain rate	f_1	f_{11}	f_{12}	f_{44}
Quasi-static	−2.96E−03	7.91E−06	−3.95E−06	4.26E−04
200 s^{-1}	−3.96E−04	3.34E−06	−1.67E−06	1.02E−04
600 s^{-1}	−2.70E−04	2.76E−06	−1.38E−06	7.30E−05
1000 s^{-1}	−3.90E−04	2.45E−06	−1.22E−06	7.02E−05

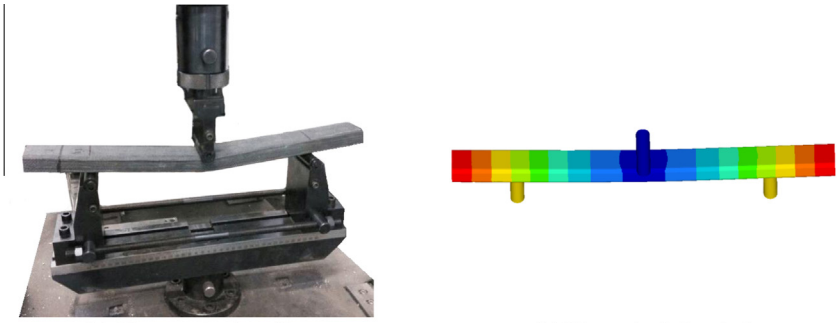

(a) Three point bending test (b) Numerical simulation

Fig. 2. Schematic illustration of experimental and numerical results of three point bending test.

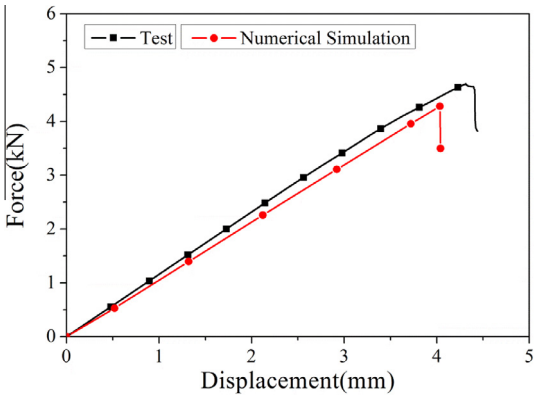

Fig. 3. Comparison of force–displacement curves between three point bending test and numerical simulation.

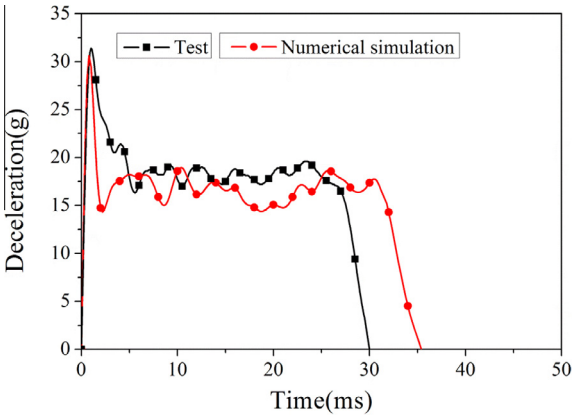

Fig. 5. Comparison of deceleration–time curves between impact test and numerical simulation.

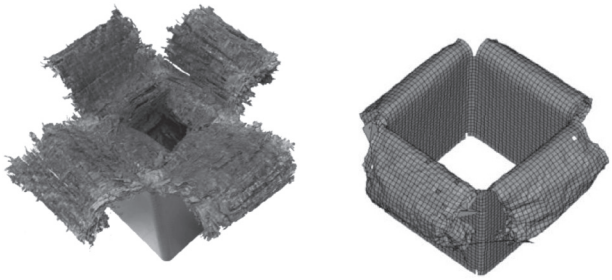

(a) Drop weight impact test (b) Numerical simulation

Fig. 4. Schematic illustration of experimental and numerical results of drop weight impact test: (a) drop weight impact test; (b) numerical simulation.

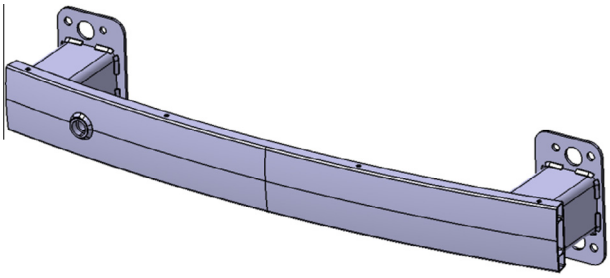

Fig. 6. The profile of the original bumper.

3. Definition of the frontal bumper beam and numerical modeling

3.1. Geometrical design of the bumper beam system

The original bumper system is manufactured by aluminum material with weight as 2.66 kg. Its main components are bumper beam, crash box, back panel and tow hook block which are assembled with each other by welding (see Fig. 6).

The bumper beam and crash box are integrated by mechanical fastening methods (welding, bolting etc.) in conventional bumper system with metallic material, but for composite bumper system, the application of mechanical fastening schemes will trigger an early detachment between the bumper beam and crash box due to the brittle failure modes of composite material [5]. New design conceptions should be developed for the purpose of maximizing the advantages derived from the composite material. In this paper, an integrated bumper system as illustrated in Fig. 7 is studied in consideration of the features of the composite material. There are mainly three parts, bumper beam, tow hook block and foam absorber. The bumper beam assembled with crash box is an enclosed construction with foam inside. The tow hook block is required to amount the hook to assist the trapped car going out of the predicament. In this research, it is designed using aluminum alloy material and is pre-embedded into the bumper beam. For structure integrality, the external surfaces of the tow hook component are wrapped by carbon fiber composite material. Foam EPP30 is employed as the absorber and its density is 30 kg/m^3. Fig. 8 demonstrates the hard point constraints which are involved in the bumper system assembly. A, auto-body mounting points; B, towing hook mounting points; C, assembly hole; D, buckle hole.

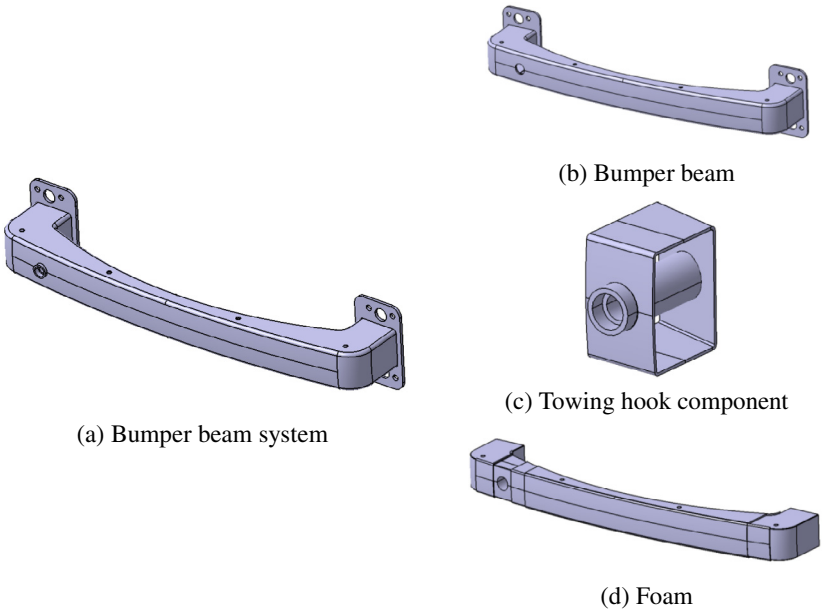

Fig. 7. The integrated bumper system: (a) bumper beam system; (b) bumper beam; (c) towing hook component; (d) foam.

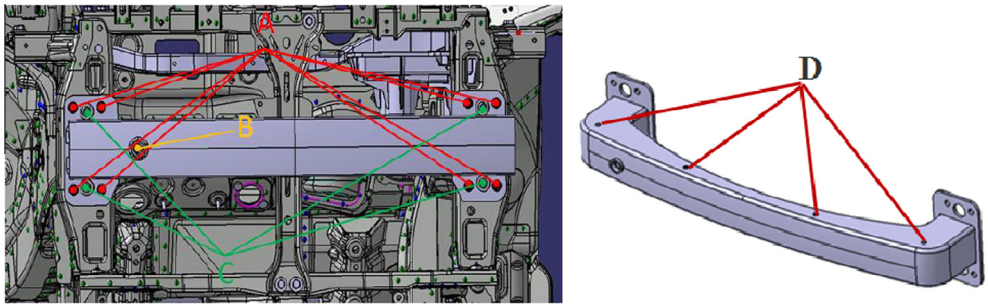

Fig. 8. The hard points constraints during the geometric design.

Five thickness variables and four shape variables are selected as optimization inputs shown in Fig. 9. Variables $X1$, $X2$, $X3$, $X4$ and $X5$ are the thickness of the corresponding areas and will be considered in the optimization procedure. For the impact process, energy absorption is the area under the force displacement curve, which is proportional to the force and the crush length. Therefore, shape variables $X6$ and $X7$, which represent the crush length, are considered in the optimization design procedure. It is widely recognized that the transition fillets illustrate relatively strong effect on the energy absorption process and deformation pattern of the bumper beam. Hence, radius variables $X8$ and $X9$ are brought into the design procedure.

3.2. Finite element modeling

The geometry modification procedure is conducted in the commercial code CATIA. HyperWoks is applied to generate the finite element model of the bumper system due to its excellent performance in mesh generation (see Fig. 10). Since the average thickness of the bumper beam is much smaller than the other dimensions, shell element is the best modeling type and its size is chosen as 5 mm. Considering the anisotropic properties of the carbon fiber composite, the bumper beam is divided into 25 parts for attaching local coordinate systems. The foam is simulated by tetrahedron elements with 5 mm mesh size, and MAT57 (*MAT_LOW_DENSITY_FOAM) is used to model its material behavior. The parts of the tow hook component are modeled by shell element except the socket with hexahedral element and all the element sizes are 5 mm. Different components are tied together in a static simulation. While in impact simulation, surface to surface tiebreak contact is defined to simulate the detachment behavior between the foam and the bumper.

The detailed material properties have been characterized in Section 2, and the simulation model is established based on classical lamination theory. Each of the ply is 0.25 mm. In the present study, the stacking sequence has not been taken into account in the optimization problem, and 45° plies have been added into the laminates to balance the mechanical performance. The laminates are assumed to be symmetric and the sequence is $[0_2/45_2/0_n/45_2/0_2]$. Fig. 11 is the schematic diagram of an 11-plys carbon fiber composite material.

3.3. Finite element simulation

In this research, strength analyses of the tow hook block, low velocity impact simulations and noise vibration and harshness (NVH) are taken into consideration.

The strength analysis is performed using implicit computing in ABAQUS. The simulation model is shown in Fig. 12. A part of the front rail is included in the model, which is fully constrained at the end during the static analysis. The loading force applied on the tow hook is 50% of the gross vehicle weight (GVW). There

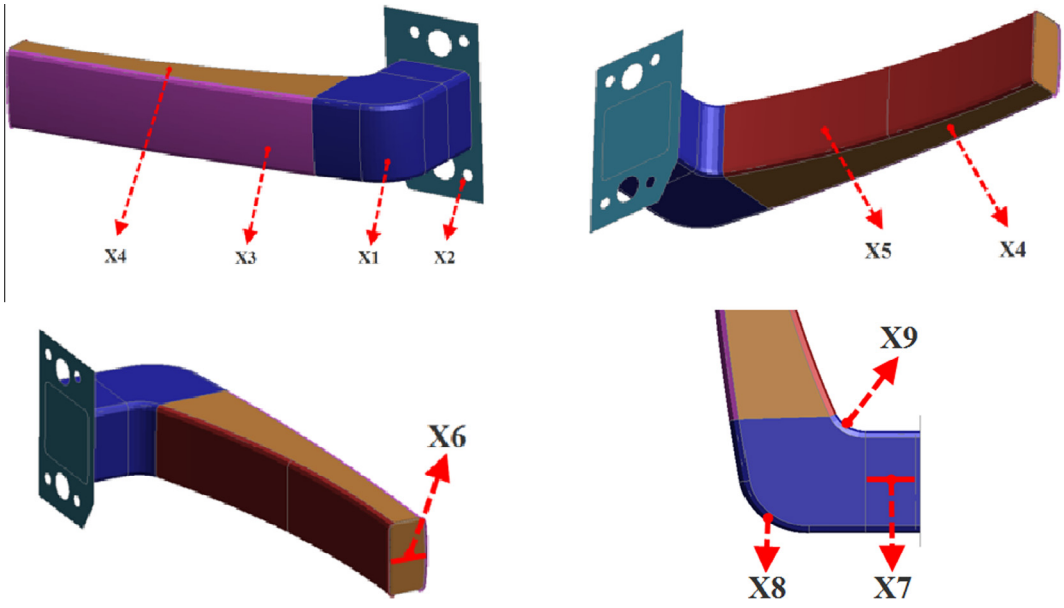

Fig. 9. The design variables of the bumper system.

(a) Bumper beam system

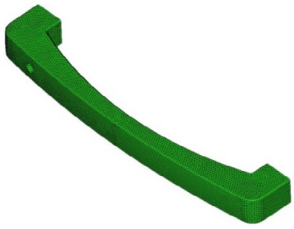

(b) Foam

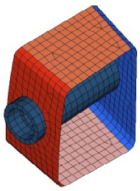

(c) Towing hook component

Fig. 10. The finite element model of the bumper beam system: (a) bumper beam system; (b) foam; (c) towing hook component.

are six load cases as shown in Table 5. Load cases 1 and 4 simulate the tension and compression conditions of the tow hook. Load cases 2, 3, 5 and 6 represent the conditions when the tow hook is loaded at certain angles. Stress results must not exceed the strength limit of the composite material with predefined safety factor.

The impact behavior of the bumper system is checked according to the conditions stated in E.C.E., Regulation No. 42, 1994 [26] and RCAR (Research Council For Automobile Repairs) regulation [27]. Low velocity impact simulations are conducted using Ls-Dyna. For E.C.E. standard, the impactor is a steel structure modeled by rigid solid elements. The impact velocity is 4.25 km/h and Fig. 13 shows the straight (perpendicular) impact situation.

Impact point is located in the 40% width of the vehicle frontal structure at the driver's side. The test velocity is set to 15 km/h and the barrier should not be deformable. Fig. 14 illustrates the simulation model.

The bumper's NVH property is computed in ABAQUS and the value of the first-order mode frequency must be more than 25 Hz.

4. Optimization procedure and results verification

As mentioned above, many load cases should be considered in the design process of the bumper system. In this research, static strength analyses and dynamic impact simulations are combined together to conduct the structural optimization procedure. A technological methodology for the design of composite bumper beam from geometrical modification to structural optimization is proposed with the application of Kriging modeling technique and a modified PSO optimizer, which will be clarified thereinafter.

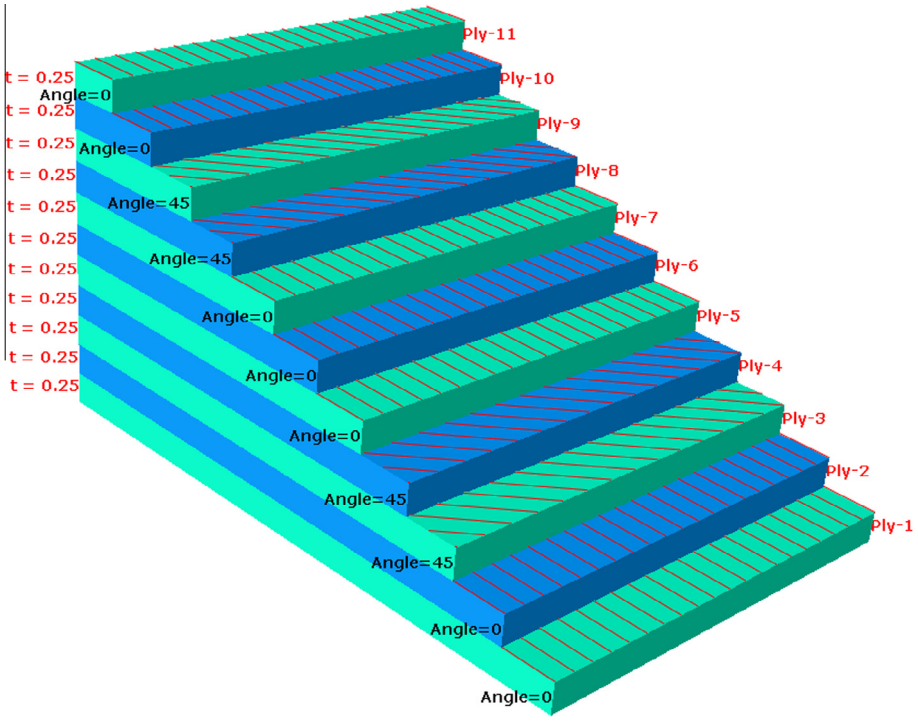

Fig. 11. Microstructure of the carbon fiber composite material.

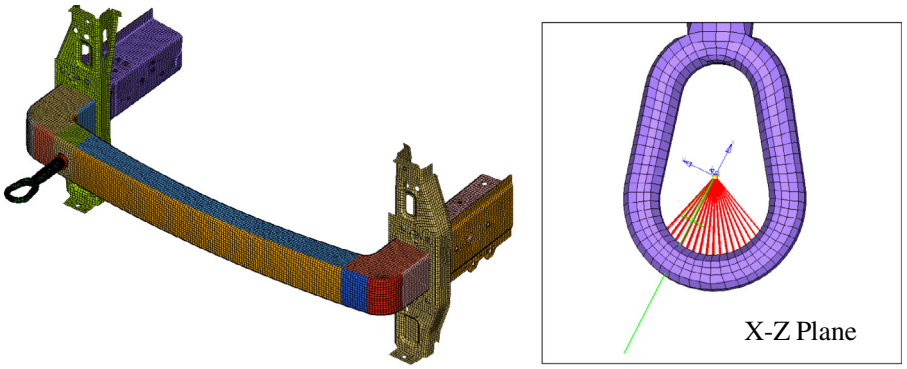

Fig. 12. Strength analysis models of the towing hook component.

Table 5
Strength analysis cases of the towing hook component.

Load cases	Loading force	Loading direction
Load case 1	−50% GVW	*X* axis positive
Load case 2	−50% GVW	5° to horizontal (down) and +25° to *X*–*Z* plane
Load case 3	−50% GVW	5° to horizontal (down) and −25° to *X*–*Z* plane
Load case 4	50% GVW	*X* axis negative
Load case 5	50% GVW	5° to horizontal (down) and +25° to *X*–*Z* plane
Load case 6	50% GVW	5° to horizontal (down) and −25° to *X*–*Z* plane

4.1. Kriging modeling technique with sequential sampling method

Design optimization of an auto-body structure, especially under crashworthiness, is a very time consuming work. Surrogate models, also called as metamodels or approximations, are often used in place of actual simulation models [28]. Kriging is one of the most common used modeling techniques and is developed for the spatial statistics and geostatistics [29,30]. Stochastic process is utilized in the Kriging model and sample points are interpolated to estimate the trend of it by a Gaussian random function. The Kriging technique has been proved to be applicable to represent multimodal and nonlinear functions. Also, the Kriging is able to provide the estimation of prediction error which is necessary in sequential sampling approach adopted in this paper.

The global approximation model is expressed as Eq. (5) in the Kriging model.

$$Y(\mathbf{x}) = \mu + Z(\mathbf{x}) \tag{5}$$

where μ is a constant global model, vector $\mathbf{x}$ represents the design variable, $Y(\mathbf{x})$ stands for the corresponding response and $Z(\mathbf{x})$ is a stochastic process with mean zero and variance σ^2. $Z(\mathbf{x})$ creates localized deviations to assist Kriging Model generating interpolation among sample points. The covariance matrix of $Z(\mathbf{x})$ is expressed as:

$$Cov[Z(\mathbf{x}^i), Z(\mathbf{x}^j)] = \sigma^2 R; \quad i,j = 1,2,\ldots,n_s \tag{6}$$

where n_s stands for the number of sample points, R is the correlation matrix of sample points.

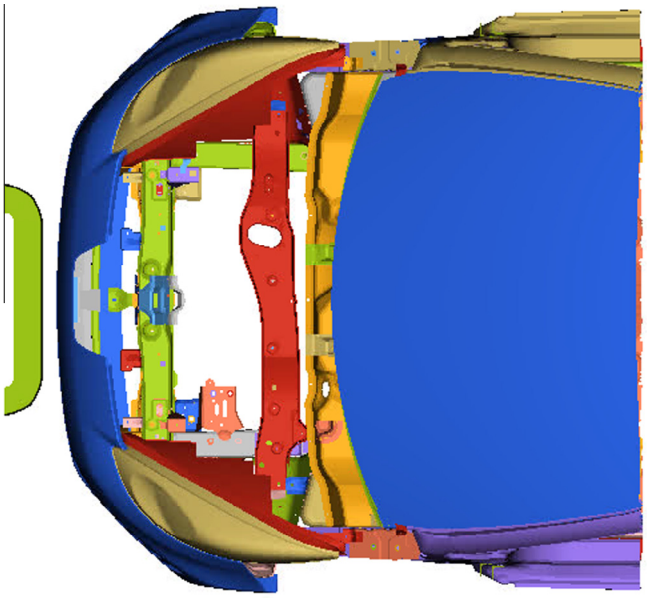

Fig. 13. Straight impact of the bumper beam system based on E.C.E. Regulation.

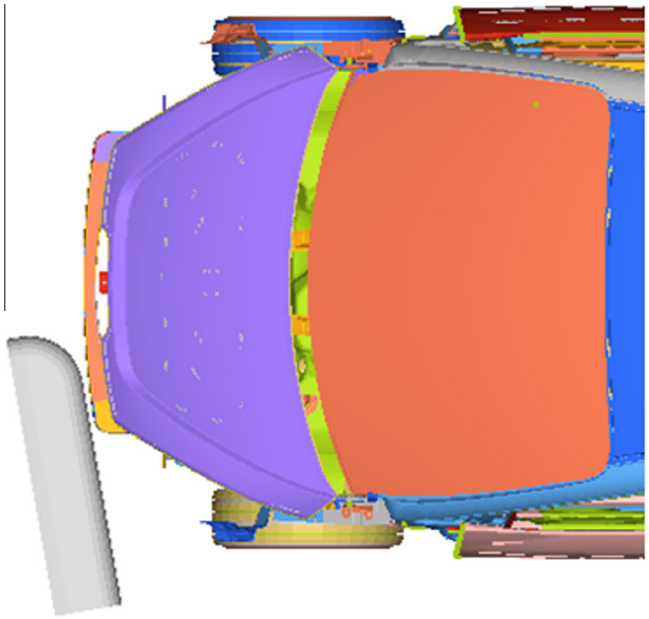

Fig. 14. RCAR test model of the bumper system.

The general form of R is:

$$R(i,j) = R(\mathbf{x}^i, \mathbf{x}^j) = \Pi_{k=1}^{n_d} \exp\left(-\theta_k |x_k^i - x_k^j|^{p_k}\right) \tag{7}$$

where $R(\mathbf{x}^i, \mathbf{x}^j)$ $(i,j = 1,2,\ldots,n_s)$ represents the correlation function between sample $\mathbf{x}^i$ and $\mathbf{x}^j$; n_d is the dimension number of the design space; $-\theta_k |x_k^i - x_k^j|^{p_k}$ is the kernel function. $\theta_k \geqslant 0$ is the unknown coefficient of correlation which is used to fit surrogate model and $0 < p_k \leqslant 2$ is defined by the type of kernel functions. Gaussian function is usually used as the kernel function and $p_k = 2$.

For given correlation θ_k and p_k, Y is predicated at an point $\mathbf{x}$ as:

$$\hat{Y}(\mathbf{x}) = \hat{\beta} + r(\mathbf{x})^T R^{-1}(Y - F\hat{\beta}) \tag{8}$$

where Y is the exact system responses; F is a unit matrix; elements in $r(\mathbf{x})$ are correlation function $R(\mathbf{x}, \mathbf{x}^i)(i = 1,\ldots,n_s)$; $\hat{\beta}$ is estimated using least squares regression:

$$\hat{\beta} = (F^T R^{-1} F)^{-1} (F^T R^{-1} Y) \tag{9}$$

Correlation parameters p_k and θ_k can be determined by the Maximum Likelihood Estimates (MLE) method.

$$\begin{aligned} &\text{Maximize}: -[n_s \ln(\hat{\sigma}^2) + \ln|R|]/2 \\ &\text{Subject to}: \begin{cases} \theta_k \geqslant 0, \\ 0 < p_k \leqslant 2, \end{cases} \quad k = 1,2,\ldots,n_d \end{aligned} \tag{10}$$

where $\hat{\sigma}^2$ is a function of θ_k and p_k:

$$\hat{\sigma}^2 = (Y - F\hat{\beta})^T R^{-1}(Y - F\hat{\beta})/n_s \tag{11}$$

The R^2 criterion is used to assess the accuracy of metamodels shown in Eq. (12). Where $\bar{y}_i$ is the mean response value of test points, $\hat{y}_i$ is the predicted response value and y_i is the real test response value.

$$R^2 = \frac{\sum_{i=1}^{n_{test}} (\hat{y}_i - \bar{y}_i)^2}{\sum_{i=1}^{n_{test}} (y_i - \bar{y}_i)^2} \tag{12}$$

The objective-oriented sequential sampling method is implemented to improve the precision of the constructed metamodels [31]. It adopts an infilling sampling criterion by defining an expected improvement (EI) function written as:

$$E[I(x)] = (y_{\min} - \hat{y}(x))\Phi\left(\frac{y_{\min} - \hat{y}(x)}{s}\right) + s\phi\left(\frac{y_{\min} - \hat{y}(x)}{s}\right) \tag{13}$$

where $y_{\min}$ is the current best function value of the obtained samples, $\hat{y}$ and s represent the predicted mean and Standard Deviation of the Kriging model at any un-sampled point, $\phi(x)$ and $\Phi(x)$ represent the probability density function and cumulative density function of a standard normal distribution, respectively. The next sampling point of x will be the point with maximum EI value.

4.2. Modified PSO optimizer

PSO (Particle Swarm Optimization), introduced by Kennedy and Eberhart [32], is a population-based optimization algorithm. The motivation of this method is derived from the imitation of cooperative behaviors among species such as fish schooling, bird flocking, etc. Potential solutions of an optimization problem are regarded as points (particles) in the design space. The PSO algorithm works on social cooperative behaviors among particles. Each particle updates its position iteratively based on its own best location and the entire swarm's best position at each generation [32–34]. Benefited from its simplicity of implementation and strong capacity of quickly finding a reasonably good solution, the PSO algorithm is becoming very popular and has been widely used in many fields.

In the standard PSO version, for a problem with D-dimensions, a potential solution can be expressed as the velocity and position of a particle. x_k^i and v_k^i represent the position and velocity of ith particle respectively. p_k^i represents the best previously visited position of each particle and p_k^g is the global best position found by the whole particle swarm. Every particle moves toward its previous best location and the global best position iteratively. The whole swarm is controlled by Eqs. (14) and (15).

$$v_{k+1}^i = \omega v_k^i + c_1 \cdot r_1 \cdot (p_k^i - x_k^i) + c_2 \cdot r_2 \cdot (p_k^g - x_k^i) \tag{14}$$

$$x_{k+1}^i = x_k^i + v_{k+1}^i \tag{15}$$

$$\omega(iter) = \frac{(iter_{\max} - iter)}{iter_{\max}} \times (\omega_{\max} - \omega_{\min}) + \omega_{\min} \tag{16}$$

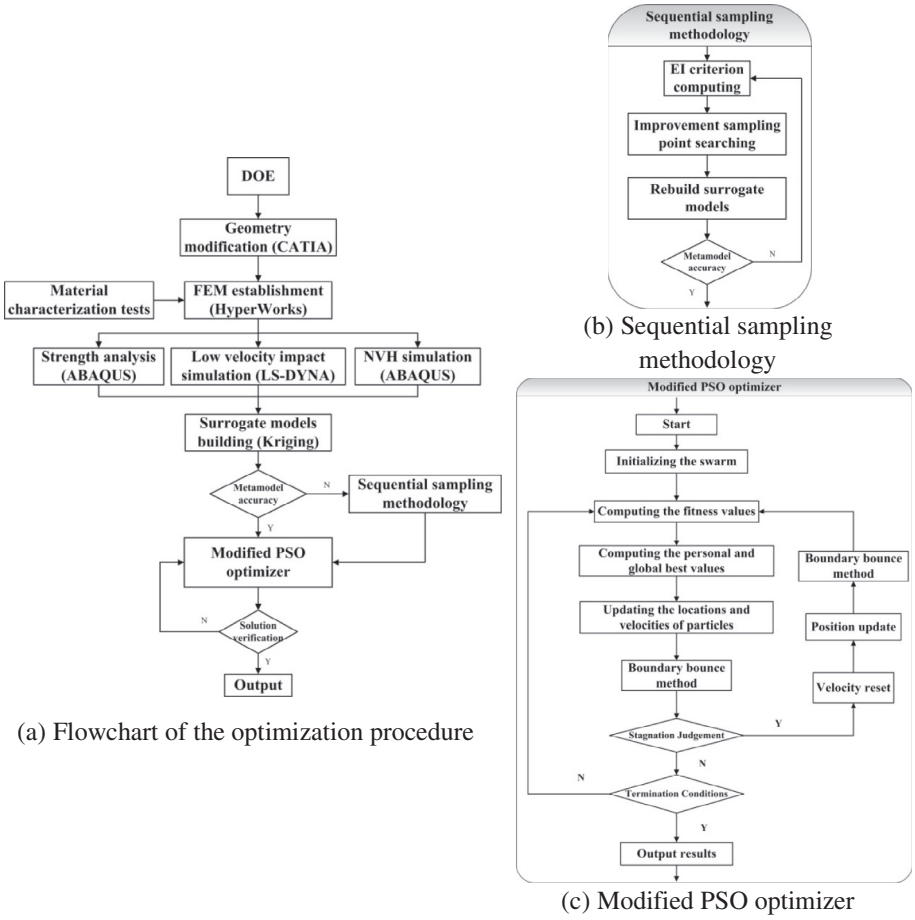

(a) Flowchart of the optimization procedure

(b) Sequential sampling methodology

(c) Modified PSO optimizer

Fig. 15. The flowchart of the proposal optimization procedure: (a) flowchart of the optimization procedure; (b) sequential sampling methodology; (c) modified PSO optimizer.

Table 6
Load cases description of the bumper system.

Load cases		Design variables	Performance indicators	Constraints
Strength simulations	Load cases 1 Load cases 2 Load cases 3 Load cases 4 Load cases 5 Load cases 6	9	Strength factor	$\leqslant$0.5
RCAR		9	Plastic strain Impact force	$\leqslant$0.07 $\leqslant$180 kN
ECE R42		9	Intrusion Impact force	$\leqslant$25 mm $\leqslant$35 kN
Mode		9	First-order torsion mode	$\geqslant$25 Hz

Eq. (14) is the velocity update equation. Its first part is the initial velocity with inertia factor ω which provides momentum for particles moving across the design space and is also used to balance the global and local search abilities during the optimization process [35]. Shi and Eberhart [36] have proposed a linearly varying inertia weight which had a significant improvement in the performance of the standard PSO, as shown in Eq. (16), in which *iter* represents the current generation and $iter_{\max}$ is the maximum generation number. The second part of Eq. (14) is named cognition component which represents the personal behavior of a particle and encourages each particle to move toward its own best previous position. The third part is called social component which stands for the cooperation behaviors among particles [37]. c_1 is named as cognitive scaling parameter and c_2 is social scaling parameter [38]. r_1 and r_2 are two uniformly distributed random numbers within the range [0,1].

The movement of particles in the PSO algorithm can result in a fast convergence rate, but it will lead to premature convergence problem because of a quick loss of diversity, which interprets the degree of dispersion among particles [39–41]. At the beginning of the optimization procedure using PSO, the diversity of the particle swarm is high after initialization. Along with the proceeding of evolution, the diversity is declined for the convergence of particles, which strengthens exploitation (local search) ability but weakens exploration (global search) capacity of the algorithm. This process is necessary at the early or middle stage of the optimization

Table 7
Kriging modeling details of multi-working conditions.

Load cases		Initial sampling points	R^2	Sequential sampling points	Improved R^2
Strength simulations	Load cases 1	70	0.9639	–	0.9639
	Load cases 2		0.9123	–	0.9123
	Load cases 3		0.7396	13	0.9315
	Load cases 4		0.9769	–	0.9769
	Load cases 5		0.9154	–	0.9154
	Load cases 6		0.7046	17	0.9163
RCAR	Plastic strain	70	0.1960	36	0.9004
	Impact force		0.7050	13	0.9127
ECE R42	Intrusion	70	0.7848	11	0.9015
	Impact force		0.8753	9	0.9214
Mode	First-order torsion mode	70	0.9973	–	0.9973

Table 8
The comparison of the optimization results.

	PSO	Modified_PSO
Problem dimension	9	9
Swarm size	20	20
Cognitive scaling parameter	2	2
Social scaling parameter	2	2
Inertia weight	0.9–0.4	0.9–0.4
Generations	100	100
Optimization results (kg)	1.937	1.686

procedure for searching effectively. However, the particles converge into a small region which leads to a very low diversity at the later stage, and that will block the further search process. Consequently, the premature convergence may occur at that time.

It is generally recognized that the lack of diversity is the dominant factor for the premature convergence problem. Mutation operators are widely used in most evolutionary optimization algorithms to prevent loss of diversity during searching process, and enable one algorithm to search a greater region of the design space. Mutation operators create variants based on current individuals, thus adding diversity to the population and avoiding stagnation of the optimization procedure in the local optima.

Through experiments with numerical benchmarks, it has been observed that PSO quickly finds a relatively good local solution but sometimes stagnates in the local optimum for a considerable number of generations without any improvement. Therefore, a modified PSO algorithm, namely OLRPSO (Optimal Latin hypercube design and an adaptive Reset operator are used to improve the standard PSO), is developed to enhance the searching capacity of the standard PSO. The OLRPSO is initialized by OLHD (Optimal Latin Hypercube Design) technique, which is one of the DOE (Design Of Experiments) techniques. DOE can be regarded as a process of identifying sampling locations in an input variable space. Mckay et al. [42] and Iman et al. [43] have proposed a widely used DOE technique, named Latin Hypercube Design (LHD) technique. Initialization stage of the PSO can be regarded as a sampling procedure, so the OLHD technique can be used to generate an initial swarm in view of its space filling property which guarantees a full coverage of a design space. After the initialization stage, a stagnation judgment criterion is employed and an adaptive reset operator working on velocity is developed to improve particle diversity in the OLRPSO algorithm. The velocity of particles will be reset by our proposed operator if the predefined probability is satisfied, when the optimization procedure is trapped into stagnation for several generations. Then the particles could have a chance to jump out from the local optimum and continue the search process. The reset operator working on the velocity update equation is shown as Eq. (17)

$$\begin{aligned} V_{reset} &= \mu \cdot rw \cdot V_{rand} \\ \mu &= \frac{(iter_{\max} - iter_{current})}{iter_{\max}} \\ rw &= (rw_{\max} - rw_{\min}) * \frac{(iter_{\max} - iter_{current})}{iter_{\max}} + rw_{\min} \end{aligned} \tag{17}$$

V_{rand} is a randomly generated velocity matrix of particles under predefined range $[-V_{\max}, V_{\max}]$. μ is a generation correlation coefficient which is linearly decreased along with generation. $iter_{\max}$ is the max generation number and $iter_{current}$ represents the current. rw is a velocity correlation coefficient which is derived from the inertia weight factor ω and its boundary is $[rw_{\min}, rw_{\max}]$. Following the searching process, the left generation number $(iter_{\max} - iter_{current})$ is decreased and the value of μ is diminished, so that the algorithm convergence property can be guaranteed by shrinking the amplitude of V_{reset}, meanwhile rw improves the distribution of reset particles with respect to the global and local searching ability. The particles are scattered away from the stagnation position by Eq. (18) after the adaptive reset operator activated.

$$P_p = P_{stagnation} + V_{reset} \tag{18}$$

There are mainly five steps during OLRPSO program:

(1) In order to guarantee a full coverage of the design space, OLRPSO is initialized by OLHD technique which is different from the standard PSO algorithm.
(2) Compute fitness values of all the particles and update their positions and velocities based on Eqs. (14) and (15).
(3) Check the predefined stagnation criterion $G_{stagnation}$ and turn into the mutation procedure conducted by the proposed velocity reset operator if the requirement is met. The stagnation criterion $G_{stagnation}$ controls the searching procedure of the algorithm. A large value of $G_{stagnation}$ will invalidate the

Table 9
Values of variables after the optimization procedure.

	$X1$	$X2$	$X3$	$X4$	$X5$	$X6$	$X7$	$X8$	$X9$
Mathematical values	4.78	5.91	3.54	2.89	2.41	36.60	52.20	50.00	22.00
Practical values	5.00	6.00	3.50	3.00	2.50	36.60	52.20	50.00	22.00

Table 10
Finite element analysis verification.

Load cases		Performance indicators	Constraints	Results
Strength simulations	Load cases 1	Strength factor	⩽0.50	0.41
	Load cases 2			0.34
	Load cases 3			0.37
	Load cases 4			0.38
	Load cases 5			0.26
	Load cases 6			0.41
RCAR		Plastic strain	⩽0.07	0.04
		Impact force	⩽180 kN	177 kN
ECE R42		Intrusion	⩽25 mm	21 mm
		Impact force	⩽35 kN	33 kN
Mode		First-order torsion mode	⩾25 Hz	240 Hz

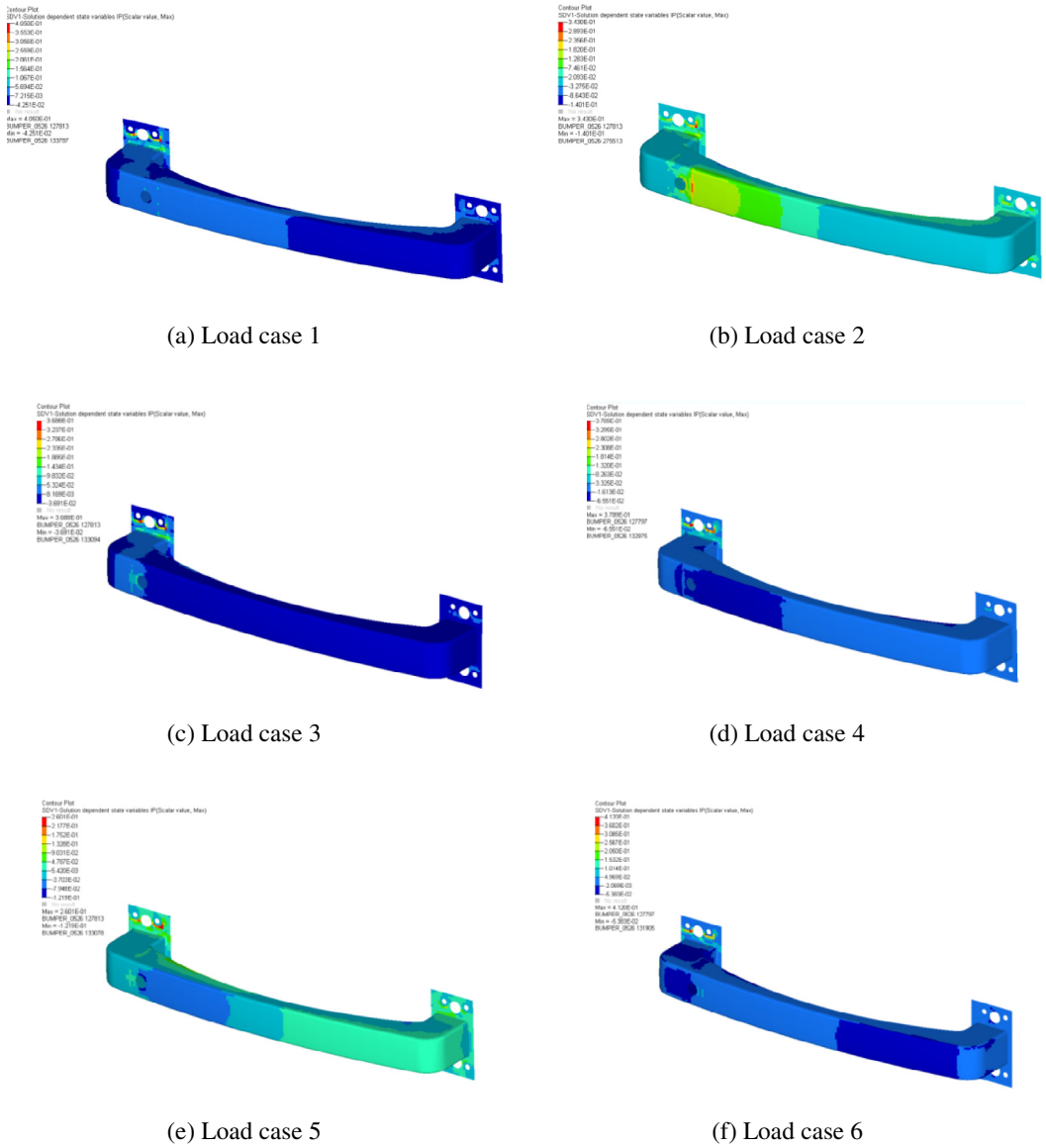

(a) Load case 1 (b) Load case 2

(c) Load case 3 (d) Load case 4

(e) Load case 5 (f) Load case 6

Fig. 16. The strength factor of each load case: (a) load case 1; (b) load case 2; (c) load case 3; (d) load case 4; (e) load case 5; (f) load case 6.

adaptive reset operator while a small value will reduce the computational efficiency. According to empirical observations, $G_{stagnation}$ is set to 5 in this article [44].

(4) In this step, the adaptive reset operator is activated. A probability P is given here to decide when the velocities and positions of particles shall be reset. It is similar to the mutation

rate used in other evolutionary algorithms and the value of 0.1 is used in this article base on empirical experiments. If the probability judgment P achieved, all the velocities and positions of particles will be reset based on Eqs. (17) and (18). So the progress stagnation can be broken up and all the particles possess the chance to find better optimization solutions. From mathematical experiments, the values of $rw_{\min}$ and $rw_{\max}$ are set to 0.1 and 0.9 respectively. From Eq. (18), the positions update of particles are based on the stagnation position, so there may have a chance that the updating particles exceed the problem boundary. From the analysis made above, boundary check program should be conducted after the reset procedure.

(5) Compute fitness values of the particles generated from step 4 and repeatedly conduct steps (2)–(4) till the termination conditions reached. The termination criterion is the predefined maximum generations in this article.

The flowchart of modified PSO method is shown in Fig. 13(c).

In order to solve the boundary of a problem, "bounce method" is used in this article [45]. If a particle moves out of the boundary, its position will be set onto the boundary and its velocity will be reversed, at each dimension i:

$$\text{If } x_{i,t+1} > x_{i,\max}, \quad \text{then } x'_{i,t+1} = x_{i,\max} \tag{19}$$

$$\text{If } x_{i,t+1} < x_{i,\min}, \quad \text{then } x'_{i,t+1} = x_{i,\min} \tag{20}$$

$$v_{i,t+1} = -v_{i,t+1} \tag{21}$$

For solving constrains in optimization problems, penalty function technique is very popular which transforms constrains into a sequence of unconstrained optimization problems. The non-stationary penalty functions, which is widely used, is employed in the present work to handle constrain functions [46].

A penalty function is generally defined as Eq. (22):

$$F(x) = f(x) + h(k)H(x), \quad x \in S \tag{22}$$

where $f(x)$ is the original objective function of the constrained problem; $h(k)$ is a modified penalty value, and k is the current iteration number; $H(x)$ is a penalty factor, represented as:

$$H(x) = \sum_{i=1}^{m} \theta(q_i(x)) q_i(x)^{\gamma(q_i(x))} \tag{23}$$

where $q_i(x) = \max\{0, g_i(x)\}$, $i = 1, \ldots, m$. $\theta(q_i(x))$ is a multi-stage assignment function. $\gamma(q_i(x))$ is the power of the penalty function and $g_i(x)$ is the constrains.

In the present work, the parameters of the penalty function are set as Yang et al. [46]. If $q_i(x) < 1$ then $\gamma(q_i(x)) = 1$, otherwise $\gamma(q_i(x)) = 2$. If $q_i(x) < 0.001$ then $\theta(q_i(x)) = 10$, else, if $q_i(x) \leqslant 0.1$ then $\theta(q_i(x)) = 20$, else, if $q_i(x) \leqslant 1$ then $\theta(q_i(x)) = 100$, otherwise $\theta(q_i(x)) = 300$. $h(k) = k\sqrt{k}$ for our optimization problem.

4.3. The optimization procedure of the bumper system

For the lightweight optimization process of the bumper system, mass minimization is the objective; constraints are constituted by the performance indicators of strength cases, low velocity impact cases and mode case. The ranges of five thickness variables are set from 1.5 mm to 6 mm, and the shape variables are designed based on the geometry constraint, shown as Eq. (24). There are eight steps to achieve the lightweight design program.

$$\begin{aligned} &\min\ M \\ &s.t.\ \ \textit{Strength cases constraints} \\ &\quad\ \textit{Low velocity impact cases constraints} \\ &\quad\ \textit{Mode constraint} \\ &\quad\ \mathbf{X}_L \leqslant \mathbf{X} \leqslant \mathbf{X}_U \\ &\quad\ \mathbf{X}_L = [1.5,\ 1.5,\ 1.5,\ 1.5,\ 1.5,\ \ 30,\ 40,\ 20,\ 10]^T \\ &\quad\ \mathbf{X}_U = [6, 6, 6, 6, 6, 70, 80, 80, 30]^T \end{aligned} \tag{24}$$

(1) Generate sampling points based on a OLHD (Optimal Latin hypercube design) technique developed by Jin et al. [47].
(2) Modify shape variables introduced in Section 3 by the CATIA commercial software based on the DOE sampling results.
(3) Import geometric models achieved in step (2), and generate high-quality mesh elements. Based on the DOE results obtained in step (1), set the corresponding thickness values and define the CFRP material.
(4) Compute the strength properties and NVH properties of the bumper system in ABAQUS and the low-velocity impact simulations in Ls-Dyna.
(5) Define inputs (DOE) and outputs (computing results from step (4)) to constitute the data structure demanded by the Kriging technique, and build the surrogate model corresponding to each load case.

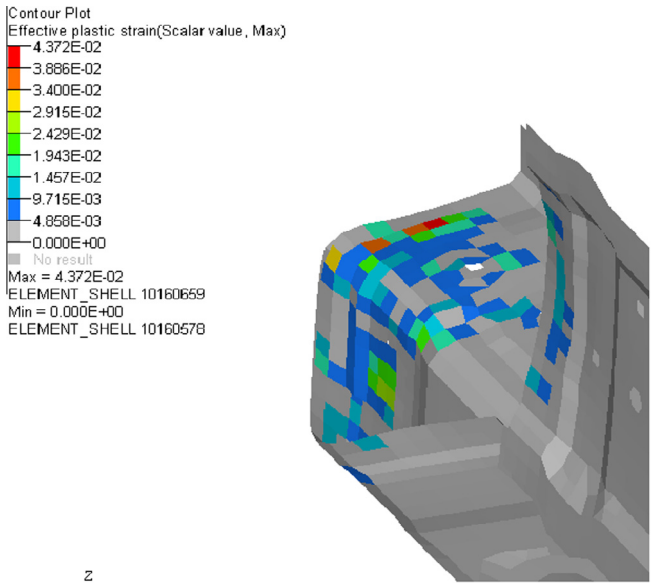

Fig. 17. The plastic strain of RCAR.

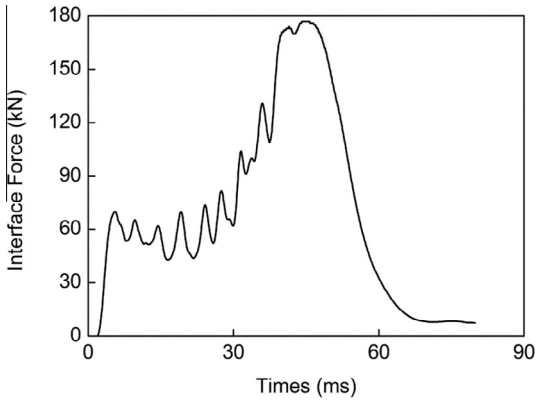

Fig. 18. The impact force of RCAR.

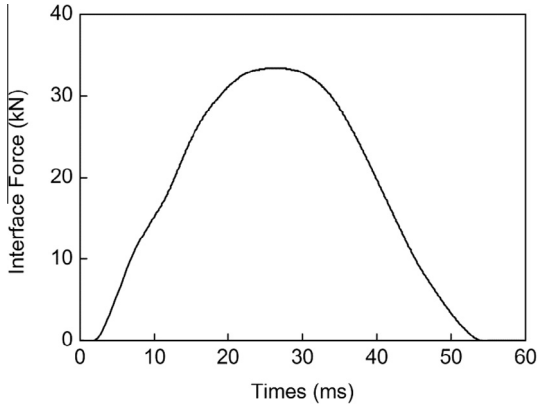

Fig. 19. The impact force of ECE R42.

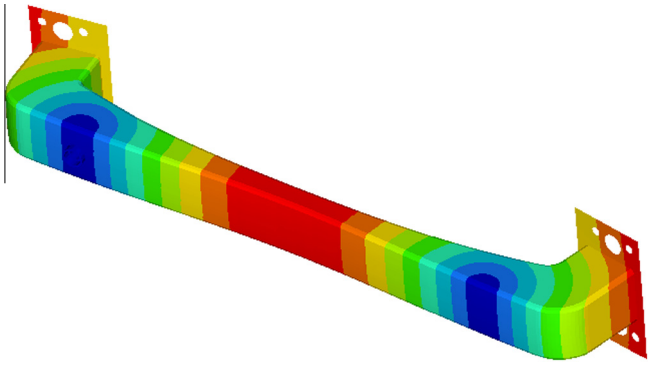

Fig. 20. The first order torsion mode.

(6) Check the accuracy of each surrogate model, and shift to sequential sampling methodology if the models dissatisfy the accuracy requirements.
(7) Search optimal solutions by modified PSO optimizer.
(8) Verify the mathematical results of finite element simulations and output optimization solutions which satisfy all requirements.

The flowchart of the proposal optimization procedure is illustrated in Fig. 15.

After the finite element models established, the Kriging modeling procedure is activated. As shown in Table 6, surrogate models corresponding to the performance indicators are built and the sequential sampling methodology is conducted based on the R^2 results illustrated in Table 7. In general, the Kriging model is confirmed as accurate when the value of R^2 is higher than 0.9. Then, the optimization searching process will be proceeded based on the relatively accurate mathematical models.

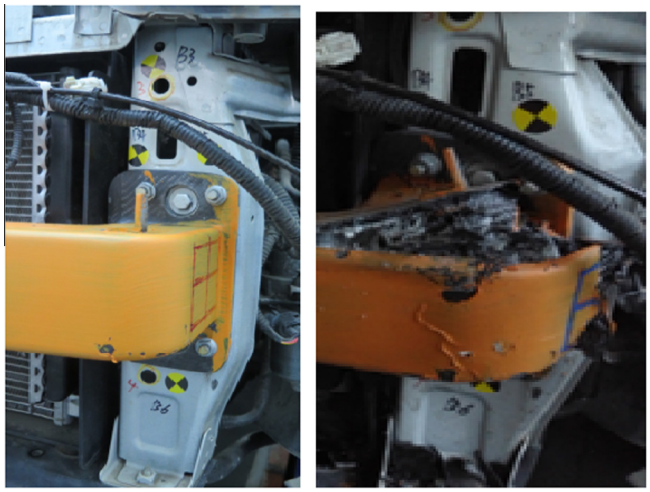

Fig. 22. The RCAR experiment of the bumper system.

The modified PSO algorithm mentioned in Section 4.2 is employed as the optimizer. In order to clarify its efficiency, a comparison case is designed between the basic and modified version. Mathematical experiments are conducted 30 times to reduce the randomness; the weight obtained from the basic version is 1.937 kg while from the modified approach is 1.686 kg which demonstrates the advantage and effectiveness of the latter (see Table 8).

Each layer is 0.25 mm, so the thickness results obtained from the mathematical searching procedure should be rounded up. In order to achieve a conservative design, the values of variables $X1$, $X2$, $X4$ and $X5$ are rounded larger than the original, shown in Table 9 and verified by finite element analysis presented in Table 10.

Figs. 15–20 are the finite element analysis results of the optimized bumper structure. The mass of the modified structure after rounded up is 1.823 kg, which is 31.5% lighter than the original structure.

The optimized bumper system was manufactured and both strength and RCAR performances have been checked. The left picture of Fig. 21 is the details of strength experiment, and it is observed that no failure happens in the composite material. The RCAR experiment is shown in Fig. 22. The optimized bumper system is mounted on a test car and the right picture of Fig. 22 is the deformation diagram after the impact process. The results of the experiment demonstrate that the optimized bumper structure satisfied the RCAR requirements.

5. Conclusions

In this paper, a structure design and optimization method considering the static strength conditions and dynamic impact cases was proposed for a commercial front bumper system made by carbon fiber plain weave composite. Two core techniques, the Kriging

Fig. 21. The strength experiment of the bumper system.

modeling technique and the Particle Swarm Optimization algorithm, were employed to accomplish the optimization procedure. Based on the test results of the commercial bumper system, the following conclusions can be summarized:

- Multi-load cases and associated high computation cost restrain the proceeding of the structural optimization design, especially for crash conditions with high-nonlinearity performance and fragmentation absorption mechanism. The Kriging modeling technique is an efficient way to settle these difficulties in composite structure design.
- Compared with the basic PSO version, the modified PSO optimizer demonstrates its benefits in optimization searching process, which is more suitable for the optimization problem of the composite bumper system.
- After the optimization procedure, the new composite bumper structure achieves a 31.5% weight reduction. The real vehicle verification proves the effectiveness and efficiency of the proposed design method.

In the future work, more detailed material's parameters, such as the stacking sequence of composite laminate plates, will be considered into the optimization procedure to achieve a better optimized structure.

Acknowledgments

The research leading to the above results was supported by National Natural Science Foundation of China (Grant No. 11372181). The authors also thank Science and Technology Commission of Shanghai Municipality (Grant No. 12521102203) and the Open Project of the State key Laboratory of Automobile Lightweight which under preparation for construction (Grant No. 20130303) for providing research funding for this work.

References

[1] Anon. European new car assessment program. <http://www.euroncap.com/(February 2014)>.
[2] Anon. United states new car assessment program. <http://www.globalncap.org/u-s-ncap/(February 2014)>.
[3] Anon. National highway trafficc safety administration. <http://www.nhtsa.gov/(February 2014)>.
[4] Anon. United nations economic commission for Europe, vehicle regulations. <http://www.unece.org/trans/main/welcwp29.html (February 2014)>.
[5] Belingardi G, Beyene AT, Koricho EG, Martorana B. Alternative lightweight materials and component manufacturing technologies for vehicle frontal bumper beam. Compos Struct 2015;120:483–95.
[6] Merklein M, Geiger M. New materials and production technologies for innovative lightweight construction. J Mater Process Tech 2002;125–126:532–6.
[7] Fuchs ERH, Field FR, Roth R. Strategic materials selection in the automobile body: economic opportunities for polymer composite design. Compos Sci Technol 2008;68:1989–2002.
[8] Hosseinzadeh Ramin, Shokrieh Mahmood M, Lessard Larry B. Parametric study of automotive composite bumper beams subjected to low-velocity impacts. Compos Struct 2005;68:419–27.
[9] Davoodi MM, Sapuan SM, Ahmad D, Ali Aidy, Khalina A, Jonoobi Mehdi. Mechanical properties of hybrid kenaf/glass reinforced epoxy composite for passenger car bumper beam. Mater Des 2010;31:4927–32.
[10] Davoodi MM, Sapuan SM, Ahmad D, Ali Aidy, Khalina A, Jonoobi Mehdi. Concept selection of car bumper beam with developed hybrid bio-composite material. Mater Des 2011;32:4857–65.
[11] Belingardi Giovanni, Beyene Alem Tekalign, Koricho Ermias Gebrekidan. Geometrical optimization of bumper beam profile made of pultruded composite by numerical simulation. Compos Struct 2013;102:217–25.
[12] Jacob GC, Fellers JF, Simunovic S, Starbuck JM. Energy absorption in polymer composites for automotive crashworthiness. J Compos Mater 2002;36(7):813–50.
[13] Mamalis A, Robinson M, Manolakos D, Demosthenous G, Ioannidis M, Carruthers J. Crashworthy capability of composite material structures. Compos Struct 1997;37(2):109–34.
[14] Carruthers J, Kettle A, Robinson A. Energy absorption capability and crashworthiness of composite material structures: a review. Appl Mech Rev 1998;51(10):635.
[15] Chen X, Li Y, Zhi Z, Guo Y, Ouyang N. The compressive and tensile behavior of a 0/90 C fiber woven composite at high strain rates. Carbon 2013;61:97–104.
[16] Hosur MV, Alexander J, Jeelani S, Vaidya UK, Mayer A. High strain compression response of affordable woven carbon/epoxy composites. J Reinf Plast Compos 2003;22:271–96.
[17] Oya N, Johnson DJ. Longitudinal compressive behavior and microstructure of PAN-based carbon fiber. Carbon 2001;39:635–45.
[18] Soden PD, Hinton MJ, Kaddour AS. A comparison of the predictive capabilities of current failure theories for composite laminates. Compos Sci Technol 1998;58(7):1225–54.
[19] Karkkainen RL, Sankar BV, Tzeng JT. A direct micromechanical approach toward the development of quadratic stress gradient failure criteria for textile composites. J Compos Mater 2007;41(16):1917–37.
[20] Mallikarachchi HMYC, Pellegrino S. Failure criterion for two-ply plain-weave CFRP laminates. J Compos Mater 2013;47(7):1357–75.
[21] Tsai SW, Wu EM. A general theory of strength for anisotropic materials. J Compos Mater 1971;5(1):58–80.
[22] Zarei H, Kroger M, Albertsen H. An experimental and numerical crashworthiness investigation of thermoplastic composite crash boxes. Compos Struct 2008;85(3):245–57.
[23] Boria S, Pettinari S, Giannoni F. Theoretical analysis on the collapse mechanisms of thin-walled composite tubes. Compos Struct 2013;103:423–30.
[24] Obradovic J, Boria S, Belingardi G. Lightweight design and crash analysis of composite frontal energy structures. Compos Struct 2012;94:423–30.
[25] Liu Q, Lin Y, Zong Z, Sun G, Li Q. Lightweight design of carbon twill weave fabric composite body structure for electric vehicle. Compos Struct 2013;97:231–8.
[26] United Nations Agreement. Uniform provisions concerning the approval of vehicles with regards to their front and rear protective devices (bumpers, etc.). E.C.E.; 1994.
[27] RCAR Bumper Test. Issue 2.0. 2010.9.
[28] Sacks J, Welch WJ, Mitchell TJ, Wynn HP. Design and analysis of computer experiments. Stat Sci 1989;4:409–35.
[29] Simpson TW, Mistree F, Korte JJ, Mauery TM. Comparison of response surface and Kriging models for multidisciplinary design optimization. AIAA Paper 98-4755; Sept. 1998.
[30] Giunta AA, Watson LT. A comparison of approximation modeling techniques: polynomial versus interpolating models. AIAA Paper 98-4758; Sept. 1998.
[31] Jones DR, Schonlau M, Welch WJ. Efficient global optimization of expensive black-box functions. J Global Optim 1998;13(4):455–62.
[32] Kennedy J, Eberhart RC. Particle swarm optimization. In: Proceedings of the IEEE international conference on neural networks. Perth, Australia, New York: IEEE Press IV; 1995. p. 1942–8.
[33] Clerc M. The swarm and queen: Towards a deterministic and adaptive particle swarm optimization. In: Proceedings of congress on evolutionary computation. Piscataway, NJ; 1999: 1951–57.
[34] Clerc M, Kennedy J. The particle swarm: explosion, stability and convergence in a multi-dimensional complex space. IEEE Trans Evol Comput 2002;6:58–73.
[35] Shi YH, Eberhart RC. A Modified particle swarm optimizer. In: IEEE international conference on evolutionary computation. ANCHORAGE, AK; 1998: 69–73.
[36] Shi YH, Eberhart RC. Empirical study of particle swarm optimization. In: IEEE international conference on evolutionary computation. Washington, DC, USA:3;1997. 101–6.
[37] Kennedy J. The particle swarm: social adaptation of knowledge. In: IEEE international conference on evolutionary computation. Indianapolis, Indiana; 1997. 303–8.
[38] Eberhart RC, Shi Y. Particle swarm optimization: developments, applications and resources. In: IEEE international conference on evolutionary computation, Seoul, South Korea; 2001:1. 81–86.
[39] Eberhart R, Shi Y. Special issue on particle swarm optimization. IEEE Trans Evol Comput 2004;8(3):201–3.
[40] Monson CK, Seppi K. Adaptive diversity in PSO. In: Proceedings of the 8th annual conference on genetic and evolutionary computation. Seattle, WA; 2006. 59–66.
[41] Salehizadeh SMA, Yadmellat P, Menhaj MB. Local optima avoidable particle swarm optimization. In: Proceedings of the 2009 swarm intelligence symposium, Nashville, TN, USA; 2009. 16–21.
[42] McKay MD, Beckman RJ, Conover WJ. A comparison of three methods for selecting values of input variables from a computer code. Technometrics 1979;21:239–45.
[43] Iman RL, Conover WJ. Small sample sensitivity analysis techniques for computer models with an application to risk assessment. Commun Stat 1980;9(17):1749–842.
[44] Andrews Paul S. An investigation into mutation operators for particle swarm optimization. In: Proceedings of the congress on evolutionary computation, Vancouver, Canada; 2006. 1044–51.
[45] Maurice Clerc. Confinements and biases in particle swarm optimization; 2006. software available at <http://clerc.maurice.free.fr/pso/>.
[46] Yang JM, Chen YP, Horng JT, Kao CY. Applying family competition to evolution strategies for constrained optimization. Lecture notes in computer science, 1213. Springer-Verlag; 1997 [p. 201–11].
[47] Jin R, Chen W, Sudjianto A. An efficient algorithm for constructing optimal design of computer experiments. J Stat Plan Inference 2005;134:268–87.